Ivlev, Sergei I.; Buchner, Magnus R.; Karttunen, Antti J.; Kraus, Florian

Synthesis and characterization of the pyridine—bromine trifluoride (1/1) complex, [py•BrF_3]

Published in:
Journal of Fluorine Chemistry

DOI:
10.1016/j.jfluchem.2018.08.009

Published: 01/11/2018

Document Version
Early version, also known as pre-print

Synthesis and Characterization of [py·BrF_3]

Sergei I. Ivlev,[1] Magnus R. Buchner,[1] Antti J. Karttunen,[2] and Florian Kraus [*,1]

[1] Fachbereich Chemie, Philipps-Universität Marburg, Hans-Meerwein-Straße 4, 35032 Marburg, Germany

[2] Department of Chemistry and Materials Science, Aalto University, 00076 Aalto, Finland

[*] E-mail: f.kraus@uni-marburg.de

Abstract

The pyridine − bromine trifluoride (1/1) complex was synthesized and characterized. It crystallizes in the monoclinic space group *C*2/*c* with a = 6.9044(9), b = 14.769(2), c = 6.9665(9) Å, β = 111.686(9)°, V = 660.12(16) Å^3, Z = 4 at 100 K. The crystal structure consists of isolated non-planar molecules linked via C–H···F hydrogen bonds. The obtained results were confirmed by quantum chemical calculations, vibrational and NMR spectroscopy. Calculations of an isolated molecule in the gas phase showed that a planar conformation of the molecule with intramolecular C–H···F hydrogen bonds is stable.

Keywords: bromine trifluoride, pyridine, complex, crystal structure, DFT

1. Introduction

Bromine trifluoride, in spite of its extreme reactivity, was reported to be a versatile and powerful fluorinating agent for various classes of organic compounds. [1–5] In many cases the corresponding reactions feature high yields and selectivity as well as short interaction times. There are however exceptions, such as aromatic compounds, where the application of BrF_3 leads to simultaneous electrophilic bromination. This leads to the formation of mixtures of aromatic brominated and fluorinated derivatives which were often left unidentified). [6] In order to overcome this disadvantage *Rozen* and coworkers proposed to use pyridine as a soft Lewis base capable of loosely binding the BrF_3 molecule in a pyridine bromine trifluoride complex, hereinafter called [py·BrF_3], and, therefore, reduce the electrophilicity of the bromine atom. [7] [py·BrF_3] can be obtained by mixing equimolar amounts of pyridine and BrF_3 in a suitable solvent (such as $CHCl_3$ or $CFCl_3$) resulting in the formation of white [py·BrF_3] as a precipitate. This precipitate can be used directly for the synthesis of CF_2 and CF_3 groups and neither its isolation nor purification are required. [7]

To the best of our knowledge and despite its advantages, [py·BrF_3] has been mentioned so far only in three publications that were mainly exploring its synthesis and reactivity. [7–9] This fact is not surprising due to the reactivity of BrF_3 towards many organic substrates: If conducted incorrectly such reactions can easily lead to explosions. So, the fears arising from that may have hampered the development of [py·BrF_3] chemistry. Therefore, the fundamental characterization of [py·BrF_3] is still missing. In this work we report our results on the characterization of [py·BrF_3] by means of single crystal X-ray diffraction, NMR and IR spectroscopy, thermal analysis as well as solid state and gas-phase quantum chemical calculations.

2. Results and Discussion

2.1. Synthesis

The pyridine bromine trifluoride (1/1) complex was synthesized by the direct reaction of bromine trifluoride with pyridine according to equation 1 [7]:

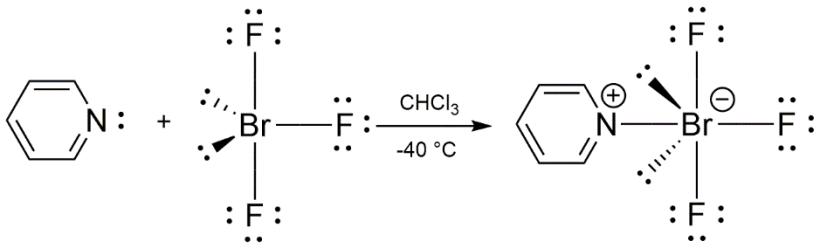

(1)

The reaction was carried out in an FEP (a copolymer of hexafluoropropylene and tetrafluoroethylene) vessel. A pre-weighed amount of BrF_3 was loaded into the vessel, cooled down to –40 °C and covered with 1 mL of precooled $CHCl_3$ or $CDCl_3$. Then, the calculated amount of pyridine was added dropwise to the reaction vessel and mixed with the frozen BrF_3. Immediately a formation of a white crystalline solid was observed. After 1 hour at –40 °C with occasional shaking the chloroform was removed by vacuum distillation at –10 °C. The white residue, [py·BrF_3], was stored in a freezer at –35 °C. At room temperature the product undergoes slow decomposition converting into a colorless liquid of so far unknown composition.

We note that the stability of solid [py·BrF_3] at room temperature has yet to be investigated. We experienced at least one explosion of approximately 300 mg of [py·BrF_3] which happened upon warming up the solid product after pumping off the solvent. The explosion severely destroyed the reaction vessel and all pieces of glassware in the vicinity. However, the explosion could be due to an unaccounted excess of BrF_3 present in the system. Frozen BrF_3 is relatively inert towards pyridine and [py·BrF_3]. But after melting (m.p. +8.8 °C) it reacts explosively and catalyzes explosive decomposition of the whole amount of [py·BrF_3] in the vessel.

2.2. Crystal structure elucidation

Inspection of the solid product that remained after evaporation of the solvent showed presence of needle-like crystals. One of them was isolated under perfluorinated oil and mounted on the goniometer of a single crystal X-ray diffractometer using the MiTeGen MicroLoops system. The results of the structure solution and refinement are shown below.

Pyridine bromine trifluoride (1/1), [py·BrF_3], crystallizes in the monoclinic space group *C*2/*c* (No. 15) with a = 6.9044(9), b = 14.769(2), c = 6.9665(9) Å, β = 111.686(9)°, V = 660.12(16) Å^3, Z = 4 at 100 K. Crystallographic details are given in Table 1. One molecule of [py·BrF_3] with the conformation obtained from the crystal structure is shown in Figure 1. A section of the crystal structure is shown in Figure 2.

Table 1. Crystallographic details for [py·BrF_3] at 100 K.

Parameter	Value
Empiric formula	$C_5H_5Br_1F_3N_1$
Color and habitus	colorless needles
Molar mass, g/mol	216.01
Crystal system	monoclinic
Space group	*C*2/*c* (No. 15)
a / Å	6.9044(9)
b / Å	14.769(2)
c / Å	6.9665(9)
β / °	111.686(9)
V / Å^3	660.12(16)
Z	4
$\rho_{calc.}$/ g cm^{-3}	2.173
μ / mm^{-1}	6.202
Crystal size / mm^3	0.133 × 0.030 × 0.019
λ / Å	0.71073 (Mo-K_α)
T / K	100
R_{int}, R_σ	0.0807, 0.0727
R(F) (all data), wR(F^2) (all data)	0.0670, 0.0831
S (all data)	1.032
No. of data points, parameters, constraints, restraints	791, 48, 3, 0
2θ range measured (min, max)	3.38, 58.86
2θ range refined (min, max)	5.52, 55.73
$\Delta\rho_{max}$, $\Delta\rho_{min}$, $\Delta\rho_{rms}$ / e·Å^{-3}	0.794, –1.065, 0.162

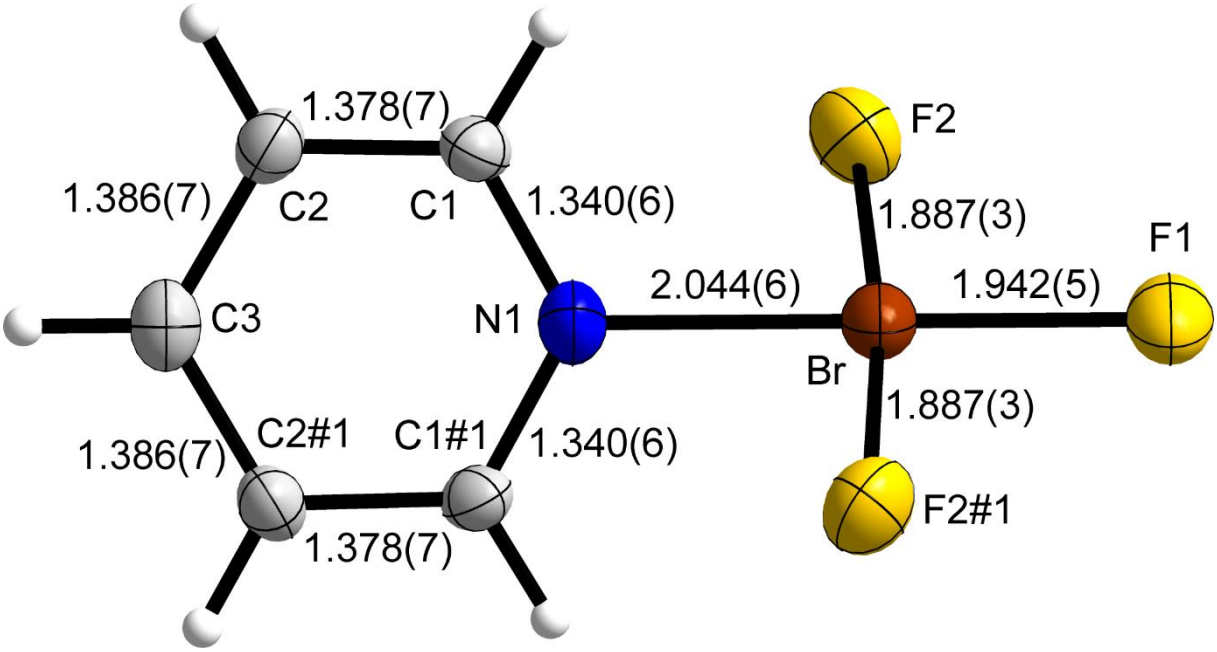

Figure 1. A molecule of [py·BrF_3] from the crystal structure. Bond lengths are given in Å. All non-hydrogen atoms are shown with anisotropic displacement ellipsoids at 70 % probability at 100 K. The hydrogen atoms are shown with arbitrary radii. Symmetry operation used for the generation of equivalent atoms: #1: 1 – *x*, *y*, 1/2 – *z*.

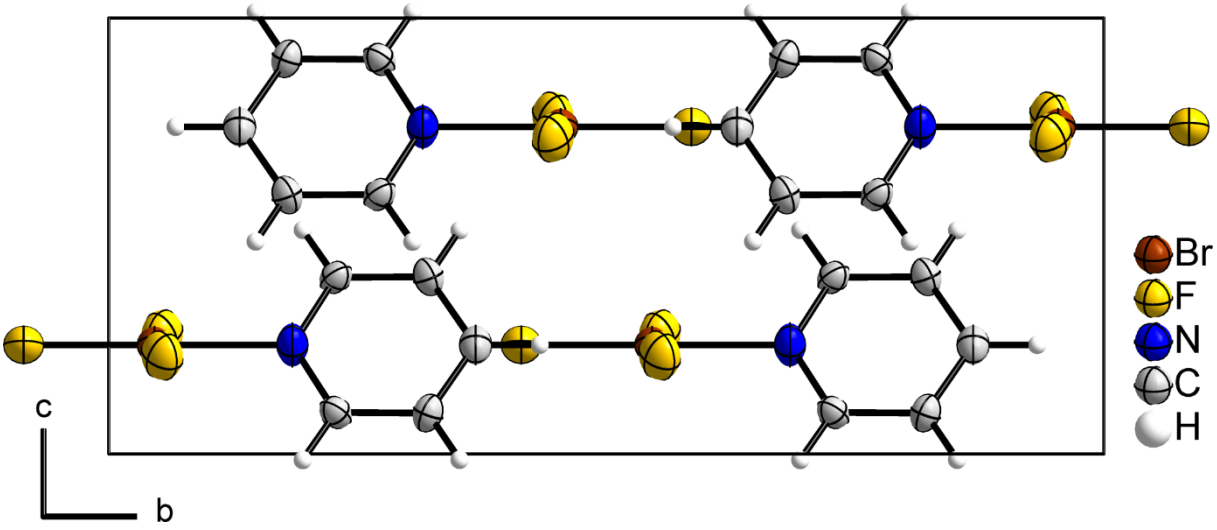

Figure 2. A section of the crystal structure of [py·BrF_3]. All non-hydrogen atoms are shown with anisotropic displacement ellipsoids at 70 % probability at 100 K. The hydrogen atoms are shown with arbitrary radii.

As seen in Figure 1, [py·BrF_3] is a Lewis acid-base complex, in which the bromine atom of bromine trifluoride is bound to the nitrogen atom of pyridine by means of halogen bonding. The Br–N bond length is 2.044(6) Å. It is of the same range as in the other nine crystallographically characterized compounds (according to the CSD database) which involve Br–$N_{aromatic}$ bonds. See Table S1 (Supporting Information) for comparison.[10–15]

The atom distances in the pyridine ring in [py·BrF_3] do not show any significant deviation from those of solid pyridine.[16] The N1–C1, C1–C2, and C2–C3 bond lengths (labelling according to Figure 1) in [py·BrF_3] equal 1.340(6), 1.378(7), and 1.386(7) Å, respectively. The corresponding average distances in pyridine are equal to 1.336, 1.381, and 1.378 Å (the estimated standard deviations are reported to lie within 0.0023 to 0.0037 Å). The angles are, however, more sensitive to the bonding of the nitrogen lone pair, and the C−N−C angle shows the strongest deviation: C1–N1–C1#1 in [py·BrF_3] equals 122.6(6)°, while in pyridine this value is only 116.6°. The other angles in [py·BrF_3] are also affected by the Br–N bond: N1–C1–C2 equals 119.6(5)°, C1–C2–C3 equals 119.2(5)°, and C2–C3–C2#1 equals 119.7(7)°. The respective angles in pyridine are equal to 123.7, 118.6, and 118.8° (the e. s. d.s reported to be within 0.16 to 0.23°).[16] Taking into account the angles, we can state that the pyridine ring in [py·BrF_3] is closer to a regular hexagon than the ring is in pure pyridine.

The bromine trifluoride molecule in [py·BrF_3] is bound to the nitrogen atom in such a manner that the coordination sphere of the Br atom is close to square planar. However, the angle between the pyridine ring plane and the BrF_3 plane equals 53.2(3)°. Therefore, the whole molecule is not planar. The square planar atomic environment around the Br atom is typical for Br in oxidation state +III and can be observed in compounds containing $[BrF_2]^+$,[17–19] $[Br_2F_5]^+$,[20,21] $[Br_3F_8]^+$ [20,21] cations, $[BrF_4]^-$,[22–27] $[Br_2F_7]^-$,[28] $[Br_3F_{10}]^-$ [28] anions, as well as in solid BrF_3.[29] The F1–Br1–N1 angle in [py·BrF_3] is exactly 180° as all three atoms reside on the crystallographic two-fold rotation axis. The F2–Br1–F2#1 angle is 172.9(2)°, the deviation from linearity is caused by the repulsion of the F2 and F2#1 atoms from the F1 atom as well as by weak intramolecular C1–H1···F2 hydrogen bonds (the H1···F2 distance equals 2.729(3) Å, the C1–H1···F2 angle equals 96.3(3)°). The resulting N1–Br1–F2 angle equals 86.47(10)°. This noticeable deviation from 90° is not typical for the square-planar $[BrF_4]^-$ anion, but can be observed in the less symmetric ions $[Br_2F_5]^+$, $[Br_3F_8]^+$, $[Br_2F_7]^-$, and $[Br_3F_{10}]^-$, where the F–F repulsion is not compensated. The bromine-fluorine distance for the F1 atom (F_{trans}) equals 1.942(5) Å, for the cis F2 and F2#1 (F_{cis}) atoms this value is 1.887(3) Å. When compared with other Br(III) compounds, these distances are found to be among the longest non-bridging F−Br bond lengths. The F_{cis}–Br bond length is close to the values reported for the $[BrF_4]^-$ anion, for example in $NaBrF_4$ 1.899(1) Å [25] and $KBrF_4$ 1.8924(9) Å. [24] The F_{trans}–Br distance is longer and lies between the values observed in the $[BrF_4]^-$ anion and the values of the Br–μ-F distance for bridging fluorine atoms in the $[Br_3F_8]^+$ cation (1.969(7) to 1.995(8) Å). [20,21]

In the crystal structure, the [py·BrF_3] molecules are held together by C–H···F hydrogen bonds (see Figure 3). The F_{trans} atom is bound to H1 atoms of two nearest molecules resulting

in a H···F distance of 2.238(3) Å and an F···C–H angle of 158.1(3)°, which indicates that these hydrogen bonds are rather strong. The F_{cis} atoms (F2) establish three weaker hydrogen bonds: two with H2 and one with H3 atoms. The resulting bond lengths and angles are the following: F2···H2: 2.586(2) and 2.629(3) Å, F2···H3: 2.390(3) Å, F2···C2–H2: 118.8(3) and 163.8(3)°, F2···C3–H3: 138.51(7)°.

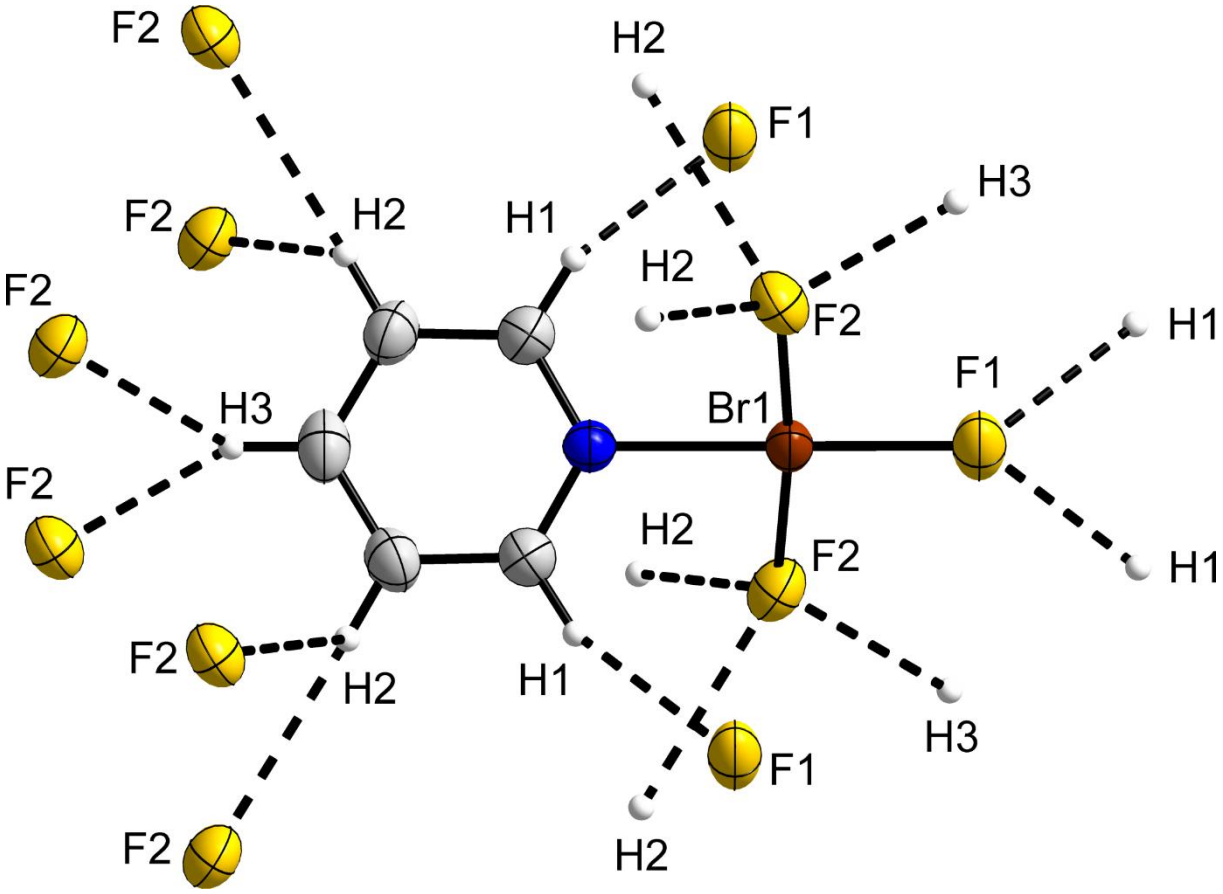

Figure 3. The hydrogen bonds in [py·BrF_3]. The intermolecular H···F bonds shorter than 3 Å are shown. The symmetry operations used for the generation of equivalent atoms are not shown for convenience. All non-hydrogen atoms are shown with anisotropic displacement ellipsoids at 70 % probability at 100 K. The hydrogen atoms are shown with arbitrary radii.

To the best of our knowledge, there are no other BrF_3 adducts with organic compounds known so far. This fact prevents us from carrying out a more detailed comparison of the observed bond lengths and angles. An appropriate candidate to compare with would be the pyridine gold trifluoride (1/1) complex, [py·AuF_3], which has been synthesized by *Riedel* and coworkers recently, but its crystal structure has not yet been reported.[30] Selected experimentally observed bond lengths, angles and cell parameters are given in Table 2. For comparison, we also give the calculated values for [py·BrF_3] in the solid state and for an isolated molecule in gas phase in Table 2 (for calculation details see below).

Table 2. Selected experimentally observed cell parameters, bond lengths and angles for [py·BrF_3] as well as the values calculated for [py·BrF_3] in the solid state and for a molecule in gas phase. The atom labels correspond to Figure 1.

Parameter	Value		
	SC XRD at 100 K	Solid state DFT at 0 K	Gas phase DFT at 0 K [c]
a / Å	6.9044(9)	7.04	–
b / Å	14.769(2)	14.45	–
c / Å	6.9665(9)	7.28	–
β / °	111.686(9)	113.9	–
V / Å^3	660.12(16)	677.4	–
N1–Br1 / Å	2.044(6)	2.05	2.26
Br1–F1$_{(trans)}$ / Å	1.942(5)	1.97	1.83
Br1–F2$_{(cis)}$ / Å	1.887(3)	1.91	1.89
N1–C1 / Å	1.340(6)	1.33	1.33
C1–C2 / Å	1.378(7)	1.38	1.38
C2–C3 / Å	1.386(7)	1.39	1.38
F2···H1 / Å [a]	2.729(3)	2.59	2.16
F1···H1 / Å [b]	2.238(3)	2.03	–
F2···H2 / Å [b]	2.586(2), 2.629(3)	2.54, 2.71	–
F2···H3 / Å [b]	2.390(3)	2.25	–
F1–Br1–N1 / °	180	180	179.9
F2–Br1–F2#1 / °	172.9(2)	171.1	172.9
C1–N1–C1#1 / °	122.6(6)	123.4	121.6
N1–C1–C2 / °	119.6(5)	119.3	120.7
C1–C2–C3 / °	119.2(5)	119.1	118.7
C2–C3–C2#1 / °	119.7(7)	119.8	119.5
C1–H1···F2 / ° [a]	96.3(3)	97.7	97.6
C1–H1···F1 / ° [b]	158.1(3)	166.1	–
C2–H2···F2 / ° [b]	118.8(3), 163.8(3)	120.9, 159.5	–
C3–H3···F2 / ° [b]	138.51(7)	133.1	–
Angle between pyridine and BrF_3 planes / °	53.7(3)	51.7	0.6

[a] Intramolecular hydrogen bond; [b] Intermolecular hydrogen bond; [c] Average values

2.3. Computational study

For better understanding of bonding in pyridine bromine trifluoride (1/1) we carried out quantum chemical DFT calculations in the CRYSTAL17 software for the solid state as well as for the gas phase.[31,32] The results of the full structural optimization are shown in Table 2.

For the solid state, our calculations are in good agreement with the experimentally determined cell parameters, bond lengths and angles. The largest discrepancy between the cell

parameters is observed for the crystallographic *c*-axis, which is overestimated by 4.5 %, but in terms of volume, however, the overestimation is only 2.6 %. Most of the calculated bond lengths correspond well to the experimentally observed ones. The only exception are the intra- and intermolecular hydrogen bonds, which were calculated pronouncedly shorter than determined by the experiment. This is, however, not a crucial warning sign since the experimentally observed hydrogen atom positions were determined using the X-ray diffraction and were refined using a riding model. We attempted to improve these results by taking into account possible dispersive interactions using the DFT-D3 method,[33] but in this case we observed strong underestimation of the cell parameters (see Table S2 in Supporting Information for details).

Interestingly, the calculations for the gas phase showed that an isolated molecule of [py·BrF_3] prefers another conformation than in the solid state (Figure 4).

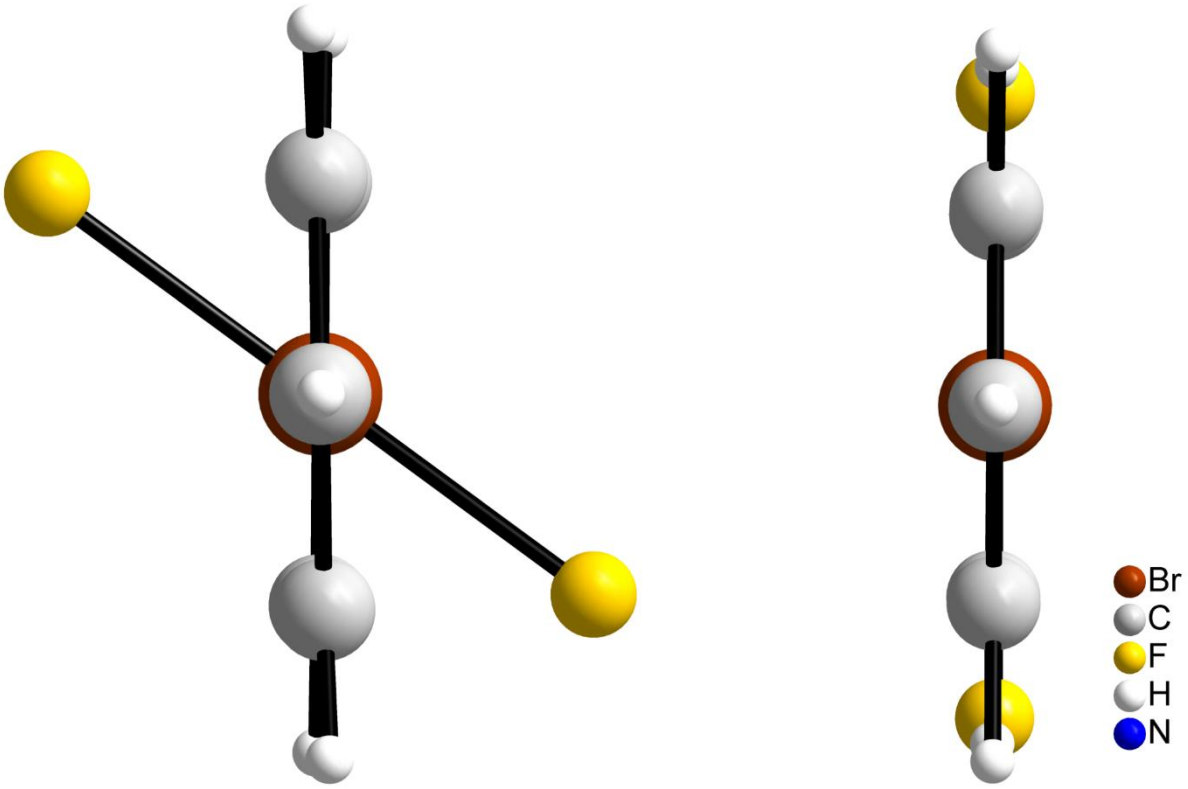

Figure 4. Comparison of the conformations of [py·BrF_3] in the solid state (left) and in the gas phase (right). Axial projection along H3–C3–N1–Br1–F1 is shown. All atoms are shown with arbitrary radii.

In the gas phase, the planes of the pyridine ring and the BrF_3 part rotate to become parallel to each other so that the whole molecule is planar. This conformation is favored due to the intramolecular F2···H1 hydrogen bonds, which are the shortest in the observed orientation and equal to 2.16 Å according to the calculations (cf.: 2.729(3) Å in solid state). This leads to the elongation of Br–N bond from 2.044(6) to 2.26 Å, and shortening of the F_{trans}–Br bond from

1.942(5) to 1.83 Å. The F_{cis}–Br bonds and the pyridine ring are essentially unaffected by the change of the conformation (see Table 2). A similar planar conformation was predicted for the likely isostructural [py·AuF_3] complex calculated at the SCS-MP2/def2-TZVPP level of theory.[30]

2.4. Vibrational spectroscopy

We characterized the title compound using IR spectroscopy and compared the obtained spectrum with the calculated one for [py·BrF_3] in the solid state (Figure 5). The assignment of the vibrational modes and their comparison with the IR bands of pyridine and bromine trifluoride are given in Table 3. The difference between the calculated spectra for [py·BrF_3] in the solid state and in the gas phase is shown in Figure S1 (Supporting Information).

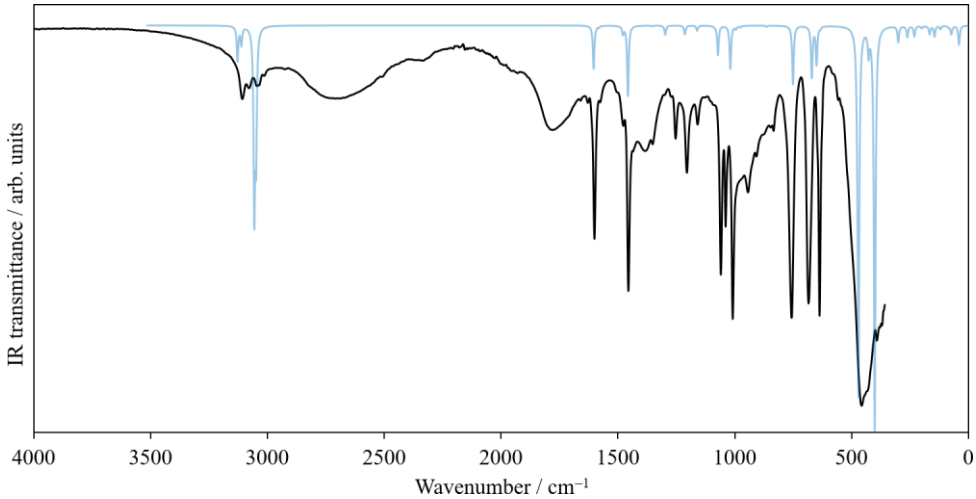

Figure 5. IR spectra of solid [py·BrF_3]. Experimentally obtained spectrum in black, calculated spectrum (solid state DFT) in blue, faded.

As seen in Figure 5, the peak positions in the calculated IR spectrum are in good agreement with the experimental data. However, the following observed broad peaks are not predicted by the theory: 2890–2480, 1890–1670, 1410–1370 cm^{-1}. A possible impurity resulting in the appearance of those peaks can be the decomposition products of [py·BrF_3] because the IR measurements were performed at room temperature. The indirect confirmation of this is the liquid state of the decomposition products, in which hydrogen bonding is likely to be present resulting in the observed broadening of the IR bands.

Comparing with the IR vibration modes of pure pyridine (Table 3), all of them are also present in [py·BrF_3].[34] The frequencies of the ring stretching and deformation bands differ only slightly indicating that the pyridine core is not drastically influenced by the BrF_3 part. The carbon-hydrogen stretching modes are more affected due to formation of hydrogen bonding

with the fluorine atoms. As a result, the carbon-hydrogen interactions decrease in strength, and the corresponding stretching frequencies undergo a bathochromic shift. The BrF_3 part of the molecule is, in contrast, highly affected by the presence of the pyridine ring. The bromine-fluorine vibration frequencies exhibit very strong bathochromic shift (~100 cm^{-1}) in comparison to pure BrF_3. The Br–F stretching modes become closer to the frequency range observed for the $[BrF_4]^-$ anion (410–580 cm^{-1}) [35] rather than to that of bromine trifluoride.[36]

The calculated IR spectrum of $[py{\cdot}BrF_3]$ in the gas phase resembles to a high degree the experimentally obtained spectrum and the one calculated for solid state (Figure S1). As expected, the strongest difference is observed for the Br–F stretching modes, which are hypsochromically shifted by circa 50 cm^{-1}. Despite that they are still in the range of the $[BrF_4]^-$ vibrations and not in that of BrF_3. As a result of the different conformation, most of the bands involving Br–N vibrations also undergo hypsochromic shift. The stronger C–H···F hydrogen bonding in the gas phase conformation results in the bathochromic shift of the C–H stretching modes.

Table 3. Experimentally observed IR bands (/ cm^{-1}) of $[py{\cdot}BrF_3]$, theoretically predicted bands for solid state and gas phase and their arbitrary intensities (in brackets). For comparison, the corresponding IR bands of pyridine and BrF_3 are given.

$[py{\cdot}BrF_3]$			BrF_3 [c] [36]	Pyridine [34]	Approximate description [d]
Experiment [a]	DFT (solid) [b]	DFT (gas) [c]			
3107 (w)	3128 (1.0)	3081 (0.1)	–	3025	C3–H3 stretch
	3111 (0.5)	3099 (0.1)		3078	C2–H2 stretch
3079 (w)	3057 (5.1)	3075 (0.8)	–	3052	C1–H1 stretch (both H1 in-phase)
3045 (w)	3048 (3.3)	3074 (0.1)	–	3033	C1–H1 stretch (both H1 out-of-phase)
1601 (s)	1603 (1.2)	1608 (0.6)	–	1581	Ring stretch + C–H scissoring
1572 (w)	1581 (<0.1)	1591 (<0.1)	–	1574	Ring stretch + C–H scissoring
1477 (s)	1477 (0.2)	1465 (0.1)	–	1482	Ring stretch + C–H rocking
1456 (m)	1456 (2.0)	1445 (1.7)	–	1437	Ring stretch + C–H rocking
1352 (m)	1356 (<0.1)	1328 (0.1)	–	1355	Ring stretch + C–H rocking
1254 (m)	1297 (0.3)	1284 (0.1)	–	1227	Ring stretch + C–H scissoring
1206 (m)	1212 (0.2)	1198 (0.9)	–	1216	Ring stretch + C–H scissoring
1160 (m)	1161 (0.1)	1137 (0.1)	–	1146	Ring stretch + C–H scissoring
1060 (s)	1089 (<0.1)	1066 (0.1)	–	1072	Ring stretch + C–H rocking
1040(s)	1071 (0.8)	1064 (0.9)	–	1068	Ring stretch + C–H rocking
	1019 (1.2)	1020 (0.1)		1030	Ring deformation (in-plane)
1010 (s)	995 (0.1)	1001 (<0.1)	–	1007	Ring deformation + H wagging
	989 (<0.1)	999 (<0.1)		991	Ring deformation + H wagging
944 (s)	974 (<0.1)	965 (<0.1)	–	984	Ring deformation + H wagging
835 (m)	863 (<0.1)	878 (<0.1)	–	881	Ring deformation + H wagging
758 (s)	750 (1.7)	753 (0.7)	–	748	Ring deformation + H wagging
685 (s)	669 (1.5)	693 (1.6)	–	701	Ring deformation + H wagging

638 (s)	649 (1.1)	632 (1.3)	–	–	Ring deformation (in-plane) + Br–N stretch
	633 (<0.1)	643 (0.1)		653	Ring deformation (in-plane)
458 (vs)	475 (1.2) 469 (10.0)	525 (8.9)	675 613	–	Symmetric F stretch Antisymmetric F stretch
436 (vs)	426 (0.7)	432 (0.3)	–	–	Ring deformation with Br–N bond
393 (vs)	400 (6.6) 399 (5.1)	–	–	–	F stretch + ring deformation F stretch + ring deformation
–	300 (0.5)	–	–	–	Deformation along F–Br–N
–	260 (0.3)	231 (0.8)	–	–	Br–N stretch
–	230 (0.3)	204 (<0.1)	–	–	Deformation along F–Br–N
–	199 (0.1)	171 (<0.1)	–	–	Deformation along F–Br–N
–	183 (<0.1)	148 (0.1)	242	–	BrF_3 rocking + Br–N stretch
–	165 (0.2)	118 (<0.1)	–	–	BrF_3 rocking
–	144 (0.3)	184 (0.1)	–	–	BrF_3 rocking
–	118 (0.1)	69 (<0.1)	–	–	BrF_3 rocking
–	84 (<0.1)	52 (<0.1)	–	–	Ring twisting
–	72 (0.2)	–	–	–	Whole molecule libration
–	65 (<0.1)	–	–	–	BrF_3 twisting
–	39 (0.5)	–	–	–	Whole molecule libration

w – weak, m – medium, s – strong, vs – very strong

[a] No bands below 360 cm^{-1} could be observed due spectrometer limitation

[b] Only IR active modes are shown

[c] Mean frequencies are given

[d] Description refers to [py·BrF_3]. Corresponding vibrations in pure pyridine and BrF_3 may slightly differ due to different atom environments

2.5. Thermal stability

Since solid [py·BrF_3] slowly decomposes already at room temperature, its thermal stability is an important question, which defines the temperature range of its applications as well as safety issues related to its handling. Visual inspection of the behavior of [py·BrF_3] during heating up to 80 °C in a closed FEP vessel showed that it rapidly converts to a brownish liquid. Upon cooling down, this appearance does not change, so this decomposition is irreversible.

To investigate this process in detail we carried out a simultaneous TG/DSC experiment to see at what temperature the decomposition occurs. The results are shown in Figure 6.

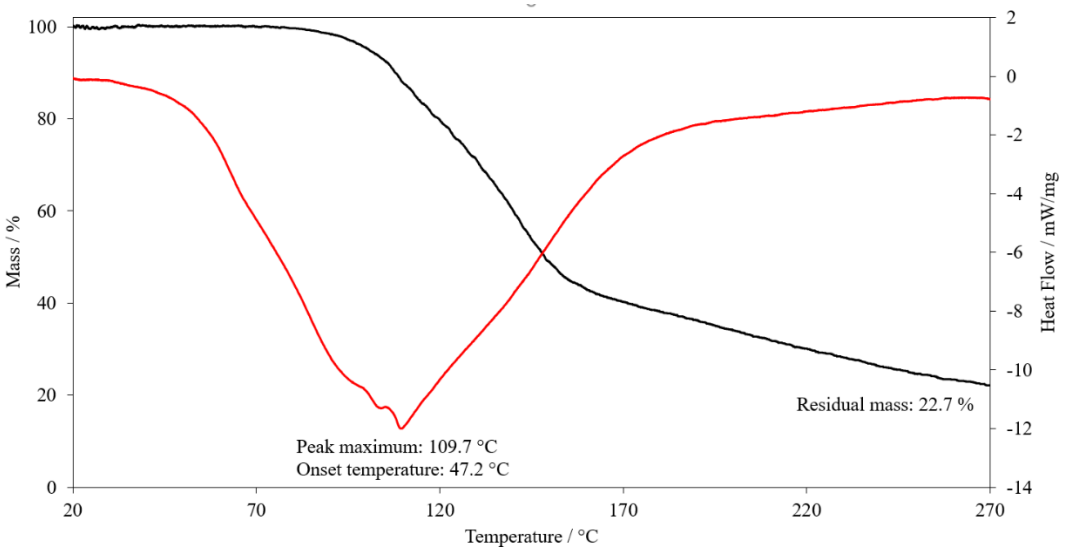

Figure 6. The TG (black) and DSC (red) curves of the thermal decomposition of [py·BrF_3] recorded at a heating rate of 10 °C/min. Exothermic effects downwards.

The results of the thermal analysis in Figure 6 show that the decomposition occurs already close to room temperature since we observe an increasing exothermic heat effect with its maximum at ~110 °C. Interestingly, there is no mass loss up to circa 100 °C, which means that the decomposition products (forming at these conditions) are not volatile. The phase of the rapid decomposition ends at ~160 °C and after that only a gradual slow mass loss can be observed. The content of the crucible after the experiment appears as a black film on the bottom and the walls visually resembling carbon. The further investigations of the decomposition process including the TG analysis coupled with mass-spectroscopy of the evolving gases and powder X-ray diffraction analysis of the final product are ongoing.

2.6. NMR Spectroscopy in solution

For the F_{cis} and F_{trans} fluorine nuclei one doublet at −31.79 ppm ($\omega_{1/2}$ = 16.0 Hz) and one triplet at 3.70 ppm ($\omega_{1/2}$ = 91.0 Hz) with a $^2J_{FF}$ coupling constant of 350.8 Hz are observed in the ^{19}F NMR spectrum of [py·BrF_3] in $CDCl_3$ at room temperature, respectively (Figure 7). These ^{19}F NMR signals are shifted considerably more downfield than those of the isostructural [py·AuF_3] (−261.1 & −267.1 ppm),[30] which is evidence for a significantly lower electron density at the ^{19}F nuclei in the BrF_3 adduct. In agreement with this is the $^2J_{FF}$ coupling constant in [py·BrF_3], which is more than one order of magnitude larger than in [py·AuF_3] (21.2 Hz).[30] In the ^{1}H NMR spectrum two triplets at 7.81 ppm ($\omega_{1/2}$ = 6.0 Hz) and 8.23 ppm ($\omega_{1/2}$ = 5.0 Hz) and one broad singlet at 8.87 ppm ($\omega_{1/2}$ = 14.5 Hz) are observed which are assigned to the ^{1}H nuclei in *meta*-, *para*- and *ortho*-position respectively (Fig. S2). These signals are all shifted

downfield compared to non-coordinated pyridine,[37] as expected, and the coordination shift is more pronounced for the protons in *ortho*- and *meta*- position than in [py·AuF_3].[30] The linewidths of all ^{1}H NMR signals in [py·BrF_3] are significantly broader than in [py·AuF_3] which is evidence for a stronger Lewis acid base adduct, resulting in slower rotation about the Br–N bond and/or stronger coupling between the hydrogen nuclei and the ^{14}N nucleus compared to the gold complex.[30] A similar line broadening is also observed for all signals in the ^{13}C NMR spectrum at 127.4 ($\omega_{1/2}$ = 8.3 Hz), 142.9 ($\omega_{1/2}$ = 3.2 Hz) and 143.7 ppm ($\omega_{1/2}$ = 3.5 Hz), which are assigned to the carbon nuclei in *para*-, *meta*- and *ortho*-position, respectively (Fig. S3). The signal of the *ortho*-carbon nuclei is split into a triplet ($^3J_{FC}$ = 5.1 Hz) due to coupling to the $^{19}F_{cis}$ nuclei, which is further evidence for the strong Br–N bond. No signals could be observed *via* ^{15}N NMR spectroscopy due to decomposition of [py·BrF_3] which is faster, than the necessary spectrum acquisition time. This decomposition is evident from the formation of new signals in the ^{1}H and ^{19}F NMR spectra of the NMR solution (see Figs. S4 & S5).

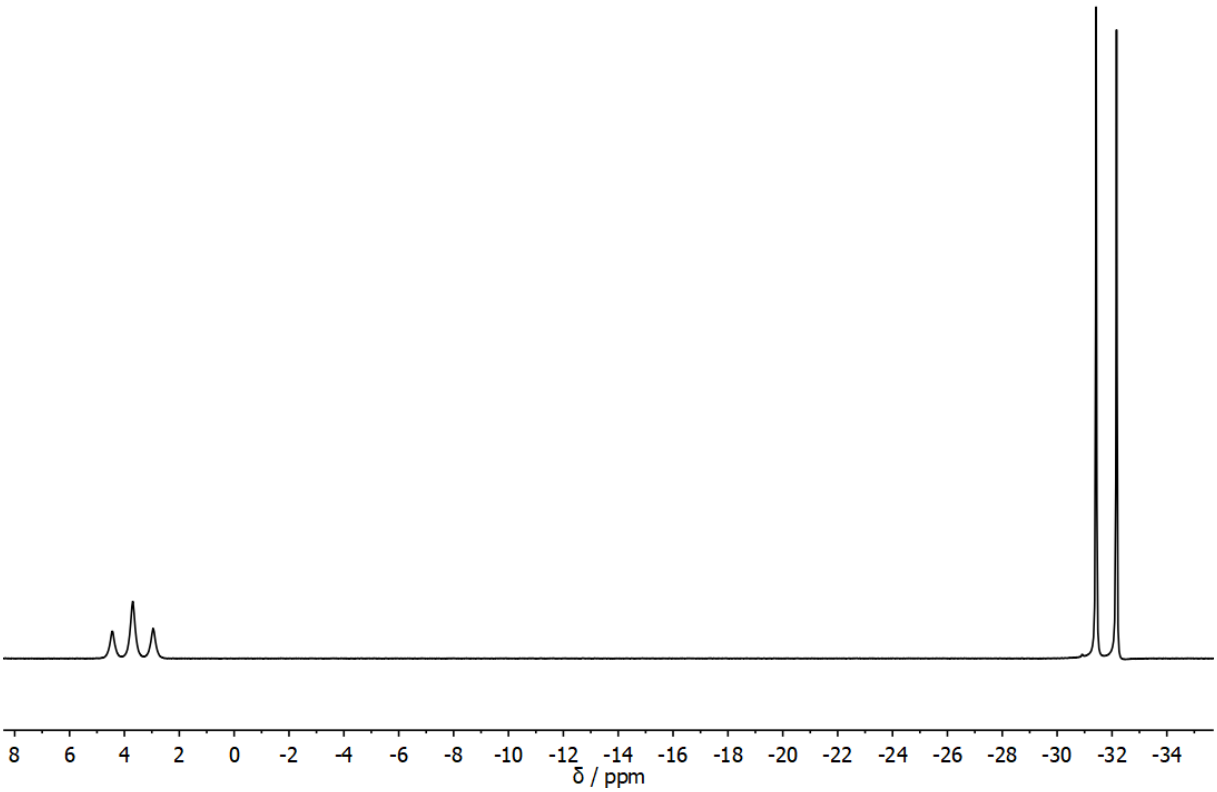

Figure 7. ^{19}F NMR spectrum of [py·BrF_3] in $CDCl_3$ at room temperature.

3. Conclusions

We have synthesized pyridine bromine trifluoride (1/1), [py·BrF_3], and characterized it using single crystal X-ray diffraction, IR-spectroscopy, ^{1}H-, ^{13}C- and ^{19}F-NMR spectroscopy as well as theoretical calculations. In the solid state the complex appears as a white crystalline

substance, which slowly decomposes at room temperature forming a colorless liquid. Depending on yet unidentified factors, the decomposition can be explosive, so appropriate safety measures must be applied for handling the compound. As shown by the TG/DTA analysis, the rate of decomposition rapidly increases with increasing temperature.

The [py·BrF_3] molecule is a Lewis acid-base complex, in which BrF_3 is attached to the nitrogen atom of the pyridine ring. In the solid state, the compound consists of single [py·BrF_3] molecules, which are held together by C–H···F hydrogen bonds. The planes through the pyridine and BrF_3 molecules are rotated with respect to each other forming an interplanar angle of 53.2(3)°. The Br–N bond length equals 2.044(6) Å at 100 K and is similar to the other crystallographically characterized aromatic complexes. The Br–F distances are equal to 1.887(3) Å (for the F_{cis} atoms) and 1.942(5) Å (for the F_{trans} atom). These values are longer in comparison to pure BrF_3 and are similar to those occurring in the $[BrF_4]^-$ anion and in the BrF_3 parts of the $[Br_3F_8]^+$ cation. The bond lengths in the pyridine ring are mostly unchanged, however, the angles are closer to 120° than in pure pyridine. These findings are supported by the vibrational spectroscopy, where we observed good correspondence between the experimentally observed and calculated IR spectra.

As shown by quantum chemical calculations, the [py·BrF_3] molecule prefers a different conformation in the gas phase in comparison to the solid state. It is then planar so that the intramolecular H···F distances are minimized.

NMR spectroscopy shows, that the dative Br−N bond in [py·BrF_3] is significantly stronger than in [py·AuF_3], which is evident from larger coupling constants, stronger coordination shifts and broader linewidths. Furthermore, the NMR data suggests that the decomposition in solution occurs within hours at ambient temperature.

4. Experimental

General: All compounds were handled in an atmosphere of dry and purified argon either in a glovebox (MBraun, Germany), or using a Monel and stainless steel Schlenk line, so that a possible contact of the substances with moisture or air was minimized (O_2 < 1 ppm, H_2O < 1 ppm). Pyridine (analytical grade) was dried stepwise with KOH and a 4 Å molecular sieve and then distilled before use. Deuterated chloroform $CDCl_3$ (euriso-top, 99.80 % D, <0.01 % H_2O) was used as delivered. BrF_3 was synthesized by slowly passing gaseous fluorine through liquid bromine (previously dried over P_4O_{10}) in a U-shaped tube (FEP, perfluorinated copolymer of ethylene and propylene) with continuous cooling.[38,39]

Synthesis of [py·BrF_3]: 87.5 mg of BrF_3 (0.64 mmol, 1 eq.) was placed in an FEP tube. The reaction vessel was cooled down to –40 °C by immersing it into cold perfluorinated oil. Then 1 mL of precooled $CDCl_3$ was added to the vessel. After 2–3 minutes 56.0 mg of cold pyridine (0.71 mmol, 1.1 eq.) was added dropwise. After stirring the formation of white precipitate was observed immediately. The vessel was kept at –40 °C for 1 hour with occasional shaking. Then the temperature was increased to –10 °C and the excess of $CDCl_3$ and pyridine was removed by several hours of evacuation. The product was kept at –35 °C in a freezer.

Elemental analysis: The carbon, hydrogen and nitrogen contents were determined with a vario MICRO cube CHN(S)-Analyzer (elementar). $C_5H_5NBrF_3$: calcd/found (%) C: 6.48 / 6.33, H 2.11 / 2.19, 27.8 / 26.15.

Single Crystal X-ray Diffraction: Structure analysis was carried out using a Stoe IPDS2T diffractometer with monochromated molybdenum radiation (Mo-Kα, λ = 0.71073 Å, a plane graphite monochromator) and an image plate detector. Evaluation and integration of the diffraction data was carried out using the Stoe X-Area software suite,[40] and a numerical absorption correction was applied. The structure was solved using direct methods (SHELXT) [41] and refined against F^2 (SHELXL) [42]. All non-hydrogen atoms were located by Difference Fourier synthesis. The hydrogen atoms were assigned and refined using a riding model. CCDC 1860887 contains the supplementary crystallographic data for this paper. These data can be obtained free of charge from The Cambridge Crystallographic Data Centre via www.ccdc.cam.ac.uk/structures.

Computational Details: The structural properties of the compounds were investigated using the CRYSTAL17 program package.[31,32] Both the atomic positions and the lattice parameters were fully optimized using the PBE0 hybrid density functional method.[43,44] Valence triple-zeta + polarization (TZVP) level (for C, N, H, F) or split-valence + polarization (SVP) level basis sets (for Br),[27,45] derived from the molecular Karlsruhe basis sets,[46] were applied (see Supporting information for additional basis set details). Additionally, we checked the significance of weak van der Waals interactions by using Grimme's D3 dispersion correction.[33] For solid state calculations the reciprocal space was sampled using a Monkhorst-Pack-type 4x4x6 k-point grid.[47] For the evaluation of the Coulomb and exchange integrals (TOLINTEG), tight tolerance factors of 8, 8, 8, 8, and 16 were used. Default optimization convergence thresholds and DFT integration grids were applied in all calculations. The harmonic vibrational frequencies,[48,49] and IR intensities,[50] were obtained by using the computational schemes implemented in CRYSTAL. The predicted spectra are based on the harmonic approximation and the wavenumbers have been scaled by a factor of 0.96 to account

for the overestimation typical for ab initio harmonic frequencies.[51] The applied scaling factor results in good agreement of the highest-energy theoretical and experimental frequencies. For the IR spectra, Gaussian line shape and FWHM of 8 cm^{-1} was used. The peak assignment was carried out by visual inspection of the normal modes in Jmol program package.[52] In addition to the solid-state calculations, we also carried out a molecular gas-phase calculation on the [py·BrF_3] molecule without any symmetry restrictions. Harmonic frequency calculation showed the gas-phase structure to be a true local minimum (XYZ coordinates are given in Supporting Information).

Thermal investigations: Simultaneous thermogravimetric and differential thermal analyses were carried out with a NETZSCH STA 409 C/CD analyzer in an Al_2O_3 crucible under argon. The crucible was covered with a tight cap with a pinhole in it. The heating rate was set to 10 °C/min using a sample mass of 2.7 mg.

IR spectroscopy: The IR spectrum was recorded using a Bruker Alpha FTIR spectrometer equipped with a diamond plate under an Ar atmosphere. The collected data were handled in the OPUS software.[53]

NMR spectroscopy: ^{1}H, ^{13}C, ^{15}N and ^{19}F NMR spectra were recorded at 300 K on a *Bruker* Avance III 500 NMR spectrometers equipped with a Prodigy Cryo-Probe. ^{1}H NMR (500 MHz) and ^{13}C NMR (126 MHz) chemical shifts are given relative to the solvent signal for $CDCl_3$ (7.26 and 77.2 ppm) while ^{15}N NMR (51 MHz) used $NH_{3(l)}$ (0 ppm) and ^{19}F NMR (471 MHz) used $CFCl_3$ (0 ppm) as an external standard respectively. Samples were sealed under inert gas into FEP tubes of 3 mm diameter. These were then put into regular glass NMR tubes (5 mm) and investigated immediately.

^{1}H NMR (500 MHz, $CDCl_3$) δ = 7.81 (t, $^{3}J_{HH}$ = 7.2 Hz, 2H, $\omega_{1/2}$ = 6.0 Hz, H_{metha}), 8.23 (t, $^{3}J_{HH}$ = 7.2 Hz, 1H, $\omega_{1/2}$ = 5.0 Hz, H_{para}), 8.87 (bs, 2H, $\omega_{1/2}$ = 14.5 Hz, H_{ortho}). ^{13}C NMR (126 MHz, $CDCl_3$) δ = 127.4 (s, $\omega_{1/2}$ = 8.3 Hz, C_{para}), 142.9 (s, $\omega_{1/2}$ = 3.2 Hz, C_{metha}), 143.7 (t, $^{3}J_{FC}$ = 5.1 Hz, $\omega_{1/2}$ = 3.5 Hz, C_{ortho}). ^{19}F NMR (471 MHz, $CDCl_3$) δ = −31.79 (d, $^{2}J_{FF}$ = 350.8 Hz, 2F, $\omega_{1/2}$ = 16.0 Hz, F_{cis}), 3.70 (t, $^{2}J_{FF}$ = 350.8 Hz, 1F, $\omega_{1/2}$ = 91.0 Hz, F_{trans}).

Acknowledgment

S.I.I. and F.K. thank the Deutsche Forschungsgemeinschaft for funding and Solvay for the generous donations of F_2. We thank Dr. Xiulan Xie of the NMR facilities and Dr. Klaus Harms of the X-ray facilities for measurement time. The work of Heike Mallinger on performing the elemental analyses is kindly acknowledged. A.J.K. thanks the CSC, the Finnish IT Center for Science, for computational resources.

References

[1] S. Rozen, *Adv. Synth. Catal.* **2010**, *352*, 2691–2707.
[2] S. Rozen, *Acc. Chem. Res.* **2005**, *38*, 803–812.
[3] L. S. Boguslavskaya, *Russ. Chem. Rev.* **1984**, *53*, 1178–1194.
[4] S. Rozen, D. Rechavi, A. Hagooly, *J. Fluorine Chem.* **2001**, *111*, 161–165.
[5] R. R. Soelch, G. W. Mauer, D. M. Lemal, *J. Org. Chem.* **1985**, *50*, 5845–5852.
[6] S. Rozen, O. Lerman, *J. Org. Chem.* **1993**, *58*, 239–240.
[7] Y. Hagooly, S. Rozen, *Org. Lett.* **2012**, *14*, 1114–1117.
[8] D. Naumann, E. Lehmann, *J. Fluorine Chem.* **1975**, *5*, 307–321.
[9] V. I. Sobolev, V. D. Filimonov, R. V. Ostvald, V. B. Radchenko, I. I. Zherin, *J. Fluorine Chem.* **2016**, *192*, *Part A*, 120–123.
[10] A. A. Neverov, H. X. Feng, K. Hamilton, R. S. Brown, *J. Org. Chem.* **2003**, *68*, 3802–3810.
[11] Y. Kim, E. J. Mckinley, K. E. Christensen, N. H. Rees, A. L. Thompson, *Cryst. Growth Des.* **2014**, *14*, 6294–6301.
[12] N. W. Alcock, G. B. Robertson, *J. Chem. Soc., Dalton Trans.* **1975**, 2483.
[13] M. Mascal, J. L. Richardson, A. J. Blake, W.-S. Li, *Tetrahedron Lett.* **1996**, *37*, 3505–3506.
[14] V. Nemec, K. Lisac, V. Stilinović, D. Cinčić, *J. Mol. Struct.* **2017**, *1128*, 400–409.
[15] D. Dolenc, B. Modec, *New J. Chem.* **2009**, *33*, 2344.
[16] D. Mootz, H. -G. Wussow, *J. Chem. Phys.* **1981**, *75*, 1517–1522.
[17] A. J. Edwards, G. R. Jones, *J. Chem. Soc. A* **1969**, *0*, 1467–1470.
[18] M. F. A. Dove, P. Benkic, C. Platte, T. J. Richardson, N. Bartlett, *J. Fluorine Chem.* **2001**, *110*, 83–86.
[19] A. J. Edwards, K. O. Christe, *J. Chem. Soc., Dalton Trans.* **1976**, *0*, 175–177.
[20] S. I. Ivlev, A. J. Karttunen, M. R. Buchner, M. Conrad, F. Kraus, *Angew. Chem.* **2018**, DOI 10.1002/ange.201803708.
[21] S. I. Ivlev, A. J. Karttunen, M. R. Buchner, M. Conrad, F. Kraus, *Angew. Chem. Int. Ed.* **2018**, DOI 10.1002/anie.201803708.
[22] W. G. Sly, R. E. Marsh, *Acta Crystallogr.* **1957**, *10*, 378–379.
[23] A. J. Edwards, G. R. Jones, *J. Chem. Soc. A* **1969**, 1936–1938.
[24] S. I. Ivlev, F. Kraus, *IUCrData* **2018**, *3*, x180646.
[25] S. I. Ivlev, R. V. Ostvald, F. Kraus, *Monatsh. Chem.* **2016**, *147*, 1661–1668.
[26] S. I. Ivlev, A. J. Karttunen, R. Ostvald, F. Kraus, *Z. Anorg. Allg. Chem.* **2015**, *641*, 2593–2598.
[27] S. Ivlev, V. Sobolev, M. Hoelzel, A. J. Karttunen, T. Müller, I. Gerin, R. Ostvald, F. Kraus, *Eur. J. Inorg. Chem.* **2014**, *2014*, 6261–6267.
[28] S. I. Ivlev, A. J. Karttunen, R. V. Ostvald, F. Kraus, *Chem. Commun.* **2016**, *52*, 12040–12043.
[29] A. M. Ellern, M. Y. Antipin, Y. T. Struchkov, V. F. Sukhoverkhov, *Russ. J. Inorg. Chem.* **1991**, *36*, 792–794.
[30] M. A. Ellwanger, S. Steinhauer, P. Golz, H. Beckers, A. Wiesner, B. Braun-Cula, T. Braun, S. Riedel, *Chem. - Eur. J.* **2017**, *23*, 13501–13509.
[31] R. Dovesi, A. Erba, R. Orlando, C. M. Zicovich-Wilson, B. Civalleri, L. Maschio, M. Rérat, S. Casassa, J. Baima, S. Salustro, et al., *WIREs Comput Mol Sci* **2018**, *8*, e1360.
[32] R. Dovesi, V. R. Saunders, C. Roetti, R. Orlando, C. M. Zicovich-Wilson, F. Pascale, B. Civalleri, K. Doll, N. M. Harrison, I. J. Bush, et al., *CRYSTAL17 User's Manual*, University Of Torino, Torino, **2017**.
[33] S. Grimme, J. Antony, S. Ehrlich, H. Krieg, *J. Chem. Phys.* **2010**, *132*, 154104.

[34] F. P. Ureña, M. F. Gómez, J. J. L. González, E. M. Torres, *Spectrochim. Acta, Part A* **2003**, *59*, 2815–2839.
[35] K. O. Christe, C. J. Schack, *Inorg. Chem.* **1970**, *9*, 1852–1858.
[36] H. Selig, H. H. Claassen, J. H. Holloway, *J. Chem. Phys.* **1970**, *52*, 3517–3521.
[37] G. R. Fulmer, A. J. M. Miller, N. H. Sherden, H. E. Gottlieb, A. Nudelman, B. M. Stoltz, J. E. Bercaw, K. I. Goldberg, *Organometallics* **2010**, *29*, 2176–2179.
[38] P. Lebeau, *Ann. Chim. Phys.* **1906**, *9*, 241–263.
[39] I. I. Gerin, *Proceedings of the 3rd International Siberian Workshop "Intersibfluorine-2006"* **2006**, 369–370.
[40] *X-Area*, Stoe & Cie GmbH, Darmstadt, Germany, **2018**.
[41] G. M. Sheldrick, *Acta Crystallogr., Sect. A: Found. Adv.* **2015**, *71*, 3–8.
[42] G. M. Sheldrick, *Acta Crystallogr., Sect. C: Struct. Chem.* **2015**, *71*, 3–8.
[43] J. P. Perdew, K. Burke, M. Ernzerhof, *Phys. Rev. Lett.* **1996**, *77*, 3865–3868.
[44] C. Adamo, V. Barone, *J. Chem. Phys.* **1999**, *110*, 6158–6170.
[45] A. J. Karttunen, T. Tynell, M. Karppinen, *J. Phys. Chem. C* **2015**, *119*, 13105–13114.
[46] F. Weigend, R. Ahlrichs, *Phys. Chem. Chem. Phys.* **2005**, *7*, 3297–3305.
[47] H. J. Monkhorst, J. D. Pack, *Phys. Rev. B* **1976**, *13*, 5188–5192.
[48] F. Pascale, C. M. Zicovich-Wilson, F. López Gejo, B. Civalleri, R. Orlando, R. Dovesi, *J. Comput. Chem.* **2004**, *25*, 888–897.
[49] C. M. Zicovich-Wilson, F. Pascale, C. Roetti, V. R. Saunders, R. Orlando, R. Dovesi, *J. Comput. Chem.* **2004**, *25*, 1873–1881.
[50] L. Maschio, B. Kirtman, R. Orlando, M. Rèrat, *J. Chem. Phys.* **2012**, *137*, 204113.
[51] A. P. Scott, L. Radom, *J. Phys. Chem.* **1996**, *100*, 16502–16513.
[52] *Jmol: An Open-Source Java Viewer for Chemical Structures in 3D. Http://Www.Jmol.Org/*, Jmol Team, **2017**.
[53] *OPUS*, Bruker Optik GmbH, Ettlingen, Germany, **2012**.